Boron Induced Crystallization of Silicon Oon Glass: An Alternate Way to Crystallize Amorphous Silicon Films for Solar Cells

SUCHETA JUNEJA
National Physical Laboratory CSIR
sushil kumar (skumar@nplindia.org)
National Physical Laboratory https://orcid.org/0000-0003-2927-1392

Research Article

Keywords: Silicon, Thin Films, Doping, Plasma Deposition, Raman Spectroscopy

Posted Date: September 22nd, 2021

DOI: https://doi.org/10.21203/rs.3.rs-894939/v1

Version of Record: A version of this preprint was published at Silicon on March 7th, 2022. See the published version at https://doi.org/10.1007/s12633-022-01738-z.

Abstract

Demand for efficient window layer in thin film solar cells with high crystallinity is ever increasing that finds important application in multi-junction/tandem silicon solar cells. Doping of diborane (B_2H_6) in hydrogenated silicon films using plasma discharge decomposition of silane (SiH_4) and (B_2H_6) gases were analyzed. The boron flow (FB) to silane ratio was varied from 0–0.30. Variation in film characteristics with B_2H_6 gas-phase ratio were analyzed, and concluded that doping boron induces crystallization in hydrogenated amorphous silicon (a-Si: H) film structure. The Raman and field emission scanning electron spectroscopy (FESEM) confirmed the boron induced crystallinity effect in silicon films at different diborane flow. The results showed that as boron content increases beyond certain ratio, silicon crystallization suppresses and the crystallite sizes were also reduced. From results, it was observed that crystallinity in FB = 0.05 is 79 % and decreases to 77 % when films are slightly higher doped (FB = 0.10) and further decreases when the films were heavily doped. These results validate that boron suppresses silicon crystallization due to local deformations caused by the impurities. Infra-red absorption studies and their analysis also confirm the crystallization in boron doped films with additional band appears at ~ 611 cm^{-1}. This band is named as boron induced crystallinity mode of vibrational spectra. The estimated hydrogen content (C_H) decreases confirmed crystallinity in the silicon structure with boron doping. Further, the energy dispersive spectroscopy (EDX) indicates the presence of boron and other impurities in deposited silicon films. The effect of boron on crystallinity and crystallite size as well as the mechanism were presented in detailed.

1. Introduction

Recently, the foremost important concern for developed (μc/nc-Si:H) micro/nano crystalline silicon materials for thin film solar cells & transistors (TFTs) [1, 2] is the growth of μc/nc-Si:H silicon on cost effective substrates at low processing temperature. In μc/nc-Si:H; high conductivity, low activation energy, high carrier mobility, high doping efficiency, high transparency, lower light absorption coefficient and high stability against light-induced degradation compared with amorphous silicon can be obtained via Boron doping [3, 4]. The extrinsic p-doped μc/nc-Si:H thin films find important application in window layer of microcrystalline silicon bottom cell of thin-film tandem (“micromorph”) solar cells [5]. P-doped micro/nanocrystalline thin films have higher transparency property hence this layer could replace silicon carbide p-type window layer in a-Si:H thin-film solar cells [6]. However, the kinetics of crystallization of a-Si films have been the focus of research area of many studies deposited by several deposition methods such as sputtering, evaporation, glow discharge, electron beam and ion –implantation has been reported [7–17]. Numerous studies consider only undoped silicon films and very few concerned and studied the effect of doping on the process of crystallization. In the past years, the consequences of n and p-type impurities in amorphized materials by ion implantation are investigated [18, 19].The several crystallization techniques involved are solid phase crystallization [20], laser anneal crystallization [21] and metal-induced crystallization [22]. However, the metal-induced crystallization method is mainly associated with metal contamination issues. Furthermore, the drawback of laser crystallization results in

the incorporation of random size of grains in amorphous silicon and the use of expensive laser in the instrument [23]. The heterogenous distribution of grain size may results voids in material/structure resulting defects in the material [24]. Therefore, plasma-enhanced chemical vapor deposition (PECVD) has been considered as the most viable low temperature doping technique for depositing silicon thin films on large area substrates.

Basically, micro/nano (μc/nc-Si: H) thin film describe as a biphasic layer, comprises of nano–sized crystallites dispersed in amorphous silicon matrix. The presence of this crystalline phase inclusions improve the structure of the films by reducing the light induced degradation effect and resulted in increasing the solar cell conversion efficiency [25]. It is also reported that the structure and properties of the films can be changed with the introduction of impurities such as doping in the material; this makes an exciting field of research [26]. For application perspective, the crystallinity of the doped layer is a key characteristic that can impact both on the doping outcome of the doped layer as well as on the intrinsic layer subsequently deposited on it. However, there are very few articles accessible related to complete study on the effect of wide range of deposition parameters on structural, electrical and optical properties all along with the correlation between the other characteristic properties of boron doped μc/nc-Si:H. In our previous investigation we mainly discussed the electrical properties with correlation among all boron doped silicon films [27]. In the present investigation, we studied a novel approach i.e. boron-dopant induced crystallization of amorphous silicon films using PECVD processing method. As per our knowledge and understanding there is no published data regarding the crystallization process occurs in silicon films via boron doping.

2. Experimental

Boron doped silicon thin films were grown using (PECVD) plasma enhanced chemical vapor deposition process. The electrode in PECVD system designed in ladder shaped geometry via VHF excitation frequency of 60 MHz. Different substrates such as Corning glass (7059), TCO coated glass and n-type double side polished silicon wafer were used at the fixed substrate temperature of 200°C and power 20 W. The substrates were cleaned using standard cleaning procedures [28]. Silanes (SiH_4) and Argon (Ar) are used as precursor gases and diborane (B_2H_6) were used as the dopant gas. The percentage of argon varied from 93.5 % to 95 % simultaneously sustaining the total pressure of chamber equals to 0.25 Torr. The diborane flow (F_B) was varied in the range from 0–0.30 where $FB = FB_2H_6/ (FSiH_4 + FA\ r + FB_2H_6)$ represent the gaseous flow rates of diborane, argon and silane respectively. The Fig. 1 represents the steps of boron doped plasma chemistry and deposition of silicon thin film on the glass substrate. The structural characteristics were analyzed with the help of (LABRAM HR 800 Horiba JY) Raman spectroscopy to calculate crystalline volume fraction (X_C) and average crystallite size. The spectra were taken in back scattering mode of geometry that is recorded at room temperature. The excitation of samples was performed through Ar^+ laser (air cooled) at 488 nm (Spectra Physics). Field emission scanning electron microscopy (FESEM) analyses were achieved using FEI electron microscope (Nova Nano SEM 450). Energy dispersive X-ray dispersive (EDX) technique was used to confirm the quantitative

analysis of boron doped silicon films. Fourier transform infra red spectroscopy (FTIR) technique were used to analyzed different configurations of silicon and hydrogen along with bonded hydrogen content (C_H) and microstructure parameter on silicon wafer substrates. The microstructure parameter (R*) has been estimated from stretching vibrational mode of spectra in deposited films.

3. Results And Discussions

3.1 Raman spectroscopy

Raman spectroscopy has been used extensively as foremost and most effective approach in analyzing structural evaluation of crystalline and amorphous silicon films [29]. The Raman spectra of different diborane doped films were taken in the wave number ranges from 350 cm^{-1} to 650 cm^{-1} and are represented in Fig. 2. From the best Lorentzian plot fitting, the spectra could be deconvoluted majorly into three different spectra covers the range 480–520 cm^{-1}: the narrow crystalline component through a lorentzian peak distribution in the region of ~ 520 cm^{-1} was allocate as TO vibrational mode of crystalline silicon or named as typical Raman spectra of crystalline silicon and the related intensities identifies as (I_c). The spectra emerges around ~ 500 cm^{-1} defined as intermediate component or attributed as Raman peak of grain boundaries and the linked intensity identifies as (I_b). A broad hump shaped distribution that arises in the region of ~ 470–480 cm^{-1} corresponds to TO vibrational mode of amorphous silicon and named as characteristic Raman spectra of amorphous silicon and the associated intensity recognized as (I_a). In calculating percentage of crystalline volume fraction; the intermediate component has to be taking into consideration as inherent portion of crystallinity. From Fig. 2, It was examined that the peak positions change from ~ 480 cm^{-1} to wave number 510 cm^{-1} with increasing diborane doping. This shift clearly reflects the transition from amorphous to crystalline phase and evidences the dopant induced crystallization in amorphous silicon matrix. From results, it was found that films deposited without doping at F_B = (0.00) shows characteristic broad hump at 480 cm^{-1} which clearly depict that the deposited film is amorphous in nature. However, the films deposited at F_B (0.05) and F_B (0.10) shows emergence of sharp crystalline TO peak at 504 and 510 cm^{-1} respectively. The Raman peak shifts to side of lower wave number as compared to single crystal silicon peak at 520 cm^{-1} suggesting that crystallites of nanometer size dimensions are dispersed in amorphous matrix. It was also observed that increasing the diborane doping favors amorphous silicon growth. This result could be explicated as boron doping effect or atomic hydrogen (H) etching effect. From the known surface diffusion model, it is recognized that the surface reaction kinetics mainly deals with the chemistry of atomic hydrogen. With increasing diborane doping, there might be large probability of configuration of B-H-Si complexes in the material structure. Further, boron related species or radicals remove atomic hydrogen from the depositing surface due to effect of ion-bombardment which might increases the number of dangling bonds on the surface and decrease the crystalline volume fraction or called as atomic boron doping amorphization effect [30].

The Raman peak were deconvoluted into three major peaks using Lorentzian distribution corresponding to crystalline and amorphous phase at around 475 and 501 cm^{-1} respectively as illustrated in Fig. 3 for the film deposited at FB = 0.05.

The crystalline volume fractions, (XC) of the deposited samples were estimated via the relation:

$$X_C = {}^{I_c}/_{I_c + I_b + I_a} \quad \text{.....(1)}$$

Where I_c, I_b and I_a defines the integrated Raman intensities analogous to crystalline, grain boundaries and amorphous phase respectively.

The crystallite size in the deposited films can be determined by using the relation:

$$D = 2\pi \sqrt{B/\Delta\omega} \quad \text{.....(2).}$$

Where Δw is the shift in nanocrystalline component to single crystal silicon peak at 520 cm^{-1} also B = 2.24 nm^2 cm^{-1} for silicon.

The size of nano-sized crystallite estimated using above relation is ~ 2 to 4 nm. The crystalline volume fraction at F_B = 0.05 is 79% and the crystalline volume fraction calculated in F_B = 0.10 is nearly 77%.

3.2 Field Emission Scanning Electron microscopy (FESEM)

To elucidate Raman results, scanning electron microscopy is carried out to examine the micro-structural evolution of amorphous and microcrystalline phase in silicon films. Scanning electron microscopy is an effective technique to investigate the morphological and topographical characteristic of the deposited silicon films.

The micrographs of FESEM images for the boron doped μc/nc-Si:H were shown in Fig. 4. It is clearly visible from the FESEM images that the micro/nanocrystalline grains are dispersed in amorphous matrix. The arrangement of crystallite structure is different at different diborane flow. Since the formation of microcrystalline silicon films initially start with an incubation layer (i.e. named as amorphous region) followed by emergence of crystalline nuclei form within the incubation layer which grows initially like nano-sized grains embedded in amorphous phase, and named as mixed phase structure. Further, these crystallites grew larger and conglomerates grain formation takes place which were named as microcrystalline silicon film.

The growth mechanism in p-type micro/nano crystalline silicon film is analogous to intrinsic micro/nanocrystalline silicon films. The density of atomic hydrogen is lower results in decreasing the diffusion probability of gas precursors on the surface. Therefore, the gas precursors were not able to

diffuse deep extent to find energetically favorable positions to form ordered structure on the surface. As a result, few were etched away and the remaining forms amorphous structure i.e. random structure. Consequently, the precursor gases which fall directly on the nuclei simply contribute to micro/nano crystalline growth [31]. From images, it is clearly observed that boron induces crystallization resulting nano-sized crystallites formation at FB = 0.05 and FB = 0.10 respectively. At higher doping ,it might assume that polyhydrides formation takes place resulting amorphization in the silicon network as observed in film deposited at FB = 0.30. The atomic boron may remove; forming other boron related species resulting increased Si-H bonding in the network. Further, these findings are well correlated with Infra-red measurements and termed as boron doping amorphization effect.

3.3 EDX (Energy dispersive X-ray spectroscopy)

EDX is a type of spectroscopy technique used for the elemental analysis, evaluation and chemical characterization of sample. In our Boron doped samples, EDX is one of the important studies. EDX spectra with associate quantities are shown in Fig. 5. With EDX spectra, we confirmed the boron doping and the presence of impurities in our silicon films like Oxygen etc. This is Quantitative analysis to confirm doping quantity in deposited silicon films. From Fig. 5, it is proved that weight % and atomic % increased with boron doping. With increase in boron doping at FB = 0.10 resulting oxygen i.e. associated with post-oxidation decreases with increased silicon content. Whereas, at FB = 0.20, boron and oxygen percentage increases but weight % of silicon decreased.

3.4 Infra-red absorption

The vibrational investigation was carried out using Fourier transform infra-red spectrometer. The Infra-red absorption spectra of deposited films are represented in Fig. 6. The FTIR spectra majorly have three absorption bands i.e. at ~ 630, 885 and 2100 cm^{-1} respectively corresponding to different modes named as wagging, bending and stretching respectively [32]. Figure 7 shows broad spectra of boron doped film deposited at FB = 0.05%. The FTIR spectra of boron doped silicon film indicates Si-Si vibrational mode which has properly defined band at ~ 611 cm^{-1}. This band is related to TO (transversal optical) with TA (transversal acoustic) mode that arises due to monocrystalline silicon substrate [32]. This mode hereby emerges and named as dopant or boron induced crystallization of the a-Si:H. This could be an alternate way to crystallize amorphous silicon. The results are in agreement with the Raman spectroscopy. The Raman spectra in Fig. 2 presented a strong/intense band with peak position centered at ~ 510 cm^{-1} i.e. longitudinal optical (LO) mode appears due to c-Si induced with diborane doping. For higher boron doped samples, the strength of this band decreases due to lack of crystallinity. Also, other characteristics of vibration modes shown in Fig. 6 disappear as the diborane doping increases. Additionally, strong absorption band examine nearly at 1060 cm^{-1} corresponds to asymmetric stretching vibration mode (Si-O-Si) in the IR spectra. This peak is an strong indication of oxidation effect due to formation of similar to porous microstructures which is a main characteristic for nc-Si:H films. Whereas, the absorption band seems at ~ 2000 cm^{-1} corresponds to vibrational stretching mode of different Si-H bonded configurations. Further with increase in doping ,the intensity of absorption band observed at ~ 630 cm^{-1}

and ~ 2000 cm^{-1} increases in the spectra (due to boron induced crystallization effect) then decreases with further doping due to amorphization effect. These consequences indicate that with increase in boron doping there might be shift in hydrogen bonding species from Si-H_2, (Si-H_2)$_n$ to Si-H bonded species or monohydride configurations.

It is already recognized that in a-Si:H ,hydrogen plays vital position in passivation of dangling bonds. This improves the optical and electrical properties due to changes in the morphology. Here, for boron doped samples, it is observed that sample with low boron doping FB = 0.05, has low Si-O intensity which relates with the electrical conductivity. From Fig. 7 we observed a vibrational bond at ~ 611 cm^{-1} in all the samples. With slight boron doping the intensity of band increases then decreases with further doping. Moreover, the band observed at ~ 2300 cm^{-1} confirmed the nanocrystalline growth via boron dopant in sample as shown in Fig. 7 for the sample FB = 0.05 %.

The FTIR spectra has been deconvoluted and from the integrated intensity of absorption peak observed at ~ 630 cm^{-1} using the empirical formulae bonded hydrogen content has been calculated [33]

$$C_H = \frac{Aw}{NSi} \int \frac{\alpha(\upsilon)}{\upsilon} \ldots\ldots\ldots\ldots\ldots\ldots\ldots\ldots\ldots\ldots\ldots\ldots\ldots\ldots\ldots (1)$$

Where α (υ) defined as the absorption coefficient of the film, (Aw) is oscillator strength whose value is equal to 2.1×10^{19} cm^{-2}, (υ) as wave number in cm^{-1} and $N_{si} = 5 \times 10^{22}$ cm^{-3} termed as material atomic density [33].

From present investigation, it can be concluded that additional band appears at ~ 611cm^{-1} is named as boron induced crystallinity mode of vibrational spectra. The Raman spectroscopy is the foremost technique in describing the crystallinity in the material (and best conductivity) which confirmed the boron induced crystallinity effect.

It is observed that initially the peak intensity observed at ~ 630 and 2100 cm^{-1} increase with boron doping then after with increasing doping, the absorption peak intensity decreases. Figure 8 illustrates the total hydrogen content and microstructure parameter with different percentage of boron doping.

With slight increase in boron doping, both hydrogen content (C_H) and microstructure parameter decreases. However, with further increase in doping percentage both hydrogen content and microstructure parameter increases as observed for FB = 0.30. The increase in hydrogen content may be due to deviation in structure from crystalline to amorphous phase as observed via Raman spectroscopy and XRD measurements as discussed in our previous published article [27]. For FB = 0.30, it was assumed that the atomic hydrogen (H) participates in the formation of Si-H bonds with the dangling bonds on the surface which diffuses in the film and eventually increases the density of SiH_3 radicals followed by gas phase reaction i.e.

$$SiH_4 + H = SiH_3 + H_2 \quad \ldots\ldots(2)$$

The hydrogen content (C_H) increases at FB = 0.30 can be ascribed to increase in hydrogen add-on next to the defect states which produced because a result of surplus boron dopant atoms that will generate micro void-rich material with increased values of R*.

4. Conclusion

Extrinsic P-doped µc/nc-Si:H films were deposited via PECVD process. From our results and analysis, it was observed that with increasing boron doping the crystalline fraction (Xc) of films decreases due to atomic boron amphorization effect. EDX studies were used to confirm the quantitative doping in the deposited films. Different bonding configurations were studied via FTIR spectroscopy. From FTIR analysis, it can be concluded that additional band in sample deposited at FB = 0.05% observed at ~ 611cm^{-1} is defined as boron induced crystallinity mode of vibrational spectra which confirmed boron induced crystallization in deposited films. These results are also well correlated with structural measurements. From SEM pictures, it is revealed that boron induces crystallization resulting nano-sized crystallites formation at FB = 0.05 and FB = 0.10 respectively. At higher boron doping there might be amorphization in the silicon network i.e. named as boron doped amorphization effect. Therefore, it can be conclude the boron doping might be an alternate approach to crystallize amorphous silicon films. High crystallinity with high conductivity boron doped µc/nc-Si:H films were used to fabricate hetero-junction diodes and these may find future important perspectives in solar cell technology.

Declarations

The manuscript has not been published elsewhere and has not been submitted simultaneously for publication anywhere.

Acknowledgements

The authors are thankful to Director, CSIR-NPL, New Delhi for their kind support and encouragement. One of the authors Sucheta Juneja acknowledges CSIR, govt. of India for providing Research Associateship (R.A.).

Author Contributions The authors have equal contributions in the paper.

Funding The authors received no financial support for the research authorship, and/or publication of this article.

Research involving Human Participants and/or Animals Not Applicable.

Data Availability My manuscript and associated personal data will be shared with Research Square to deliver the author dashboard.

Conflict of Interest The authors declare that they have no conflict of interest.

Declaration of Competing Interest The authors declare that they have no known competing financial interests or personal relationships that could have appeared to have influence the work reported in this paper.

Consent to Participate The authors consent to participate.

Consent for Publication The author's consent for publication.

References

1. Cuscunà, M., Bonfiglietti, A., Carluccio, R., Mariucci, L., Mecarini, F., Pecora, A., & Fortunato, G. (2002). *Solid-State Electronics*, *46*(9), 1351-1358.
2. Fujii, S., Fukawa, Y., Takahashi, H., Inomata, Y., Okada, K., Fukui, K., & Shirasawa, K. (2001), *65*(1-4), 269-275.
3. Saleh, R., & Nickel, N. H. (2003), *427*(1-2), 266-269.
4. Yan, W. S., Wei, D. Y., Guo, Y. N., Xu, S., Ong, T. M., & Sern, C. C. (2012). *Thin solid films*, *520*(6), 1724-1728.
5. Meillaud, F., Shah, A., Droz, C., Vallat-Sauvain, E., & Miazza, C. (2006). *Solar energy materials and solar cells*, *90*(18-19), 2952-2959.
6. [6] Das, D., & Mondal, P. (2017). *Applied Surface Science*, *416*, 980-987.
7. Limthongkul, P., Jang, Y. I., Dudney, N. J., & Chiang, Y. M. (2003). *Acta Materialia*, *51*(4), 1103-1113.
8. Brodsky, M. H., Weiser, K., & Pettit, G. D. (1970. *Physical Review B*, *1*(6), 2632.
9. Greene, J. E., & Mei, L. (1976*). Thin Solid Films*, *34*(1), 27-30.
10. Cho, G. B., Ju, J. H., Lee, W. T., Park, S. H., Ahn, H. J., Kim, K. W., .. & Nam, T. H. (2021). *Journal of Alloys and Compounds*, *860*, 158507.
11. [11] Kamins, T. (2012). *Polycrystalline silicon for integrated circuit applications* (Vol. 45). Springer Science & Business Media.
12. Nguyen, H. T. K., Hanafusa, H., Mizukawa, Y., Hayashi, S., & Higashi, S. (2021). *Materials Science in Semiconductor Processing*, *121*, 105357.
13. Ohdaira, K., Fujiwara, T., Endo, Y., Nishizaki, S., & Matsumura, H. (2009). *Journal of Applied Physics*, *106*(4), 044907.
14. Ronning, C., Borschel, C., Geburt, S., & Niepelt, R. (2010). *Materials Science and Engineering: R: Reports*, *70*(3-6), 30-43.
15. I. P. Jain, and G. Agarwal. "Ion beam induced surface and interface engineering." Surface Science Reports 66, no. 3-4, 77-172,(2011).
16. Or-Bach, Z., Cronquist, B., Beinglass, I., De Jong, J. L., Sekar, D. C., & Lim, P. (2013). *U.S. Patent No. 8,362,482*. Washington, DC: U.S. Patent and Trademark Office.

17. Greve, D. W., & Hatalis, M. K. (2021). In *Microscopy of Semiconducting Materials, 1987* (pp. 479-484). CRC Press.
18. Madou, M. J. (2018). *Fundamentals of microfabrication: the science of miniaturization*. CRC press.
19. Mokshin, P. V., Juneja, S., & Pavelyev, V. S. (2019, November). In *Journal of Physics: Conference Series* (Vol. 1368, No. 2, p. 022060). IOP Publishing.
20. Sedani, S. H., Yasar, O. F., Karaman, M., & Turan, R. (2020). *Thin Solid Films*, *694*, 137639.
21. Lien, M. T. K., & Horita, S. (2014). *Japanese Journal of Applied Physics*, *53*(3S1), 03CB01.
22. Hainey Jr, M. F., Innocent-Dolor, J. L., Choudhury, T. H., & Redwing, J. M. (2017). *Journal of Applied Physics*, *121*(11), 115301.
23. Chao, C. H., Weng, K. W., Cheng, H. L., Chan, C. H., & Lien, S. Y. (2010). *Thin solid films*, *518*(24), 7480-7482.
24. Juneja, S., Sudhakar, S., Srivastava, A. K., & Kumar, S. (2016). *Thin Solid Films*, *619*, 273-280.
25. Juneja, S., Sudhakar, S., Gope, J., & Kumar, S. (2015). *Materials Science in Semiconductor Processing*, *40*, 11-19.
26. Li, Z., Zhang, X., & Han, G. (2010). *physica status solidi (a)*, *207*(1), 144-148.
27. Juneja, S., Sudhakar, S., Gope, J., Lodhi, K., & Sharma, M. (2015). *Journal of Alloys and Compounds*, *643*, 94-99.
28. Juneja, S., Verma, P., Savelyev, D. A., Khonina, S. N., Sudhakar, S., & Kumar, S. (2016, April). In *AIP conference proceedings* (Vol. 1724, No. 1, p. 020016). AIP Publishing LLC.
29. Juneja, S., & Kumar, S. (2020). *Silicon*, 1-14.
30. Yan, X. Q., Huang, X. M., Uda, S., & Chen, M. W. (2005). *Applied Physics Letters*, *87*(19), 191911.
31. Stuckelberger, M., Biron, R., Wyrsch, N., Haug, F. J., & Ballif, C. (2017). *Renewable and Sustainable Energy Reviews*, *76*, 1497-1523.
32. Juneja, S., Sharma, M., & Kumar, S. (2019). *Silicon*, *11*(4), 1925-1937.
33. Funde, A. M., Bakr, N. A., Kamble, D. K., Hawaldar, R. R., Amalnerkar, D. P., & Jadkar, S. R. (2008). *Solar Energy Materials and Solar Cells*, *92*(10), 1217-1223.

Figures

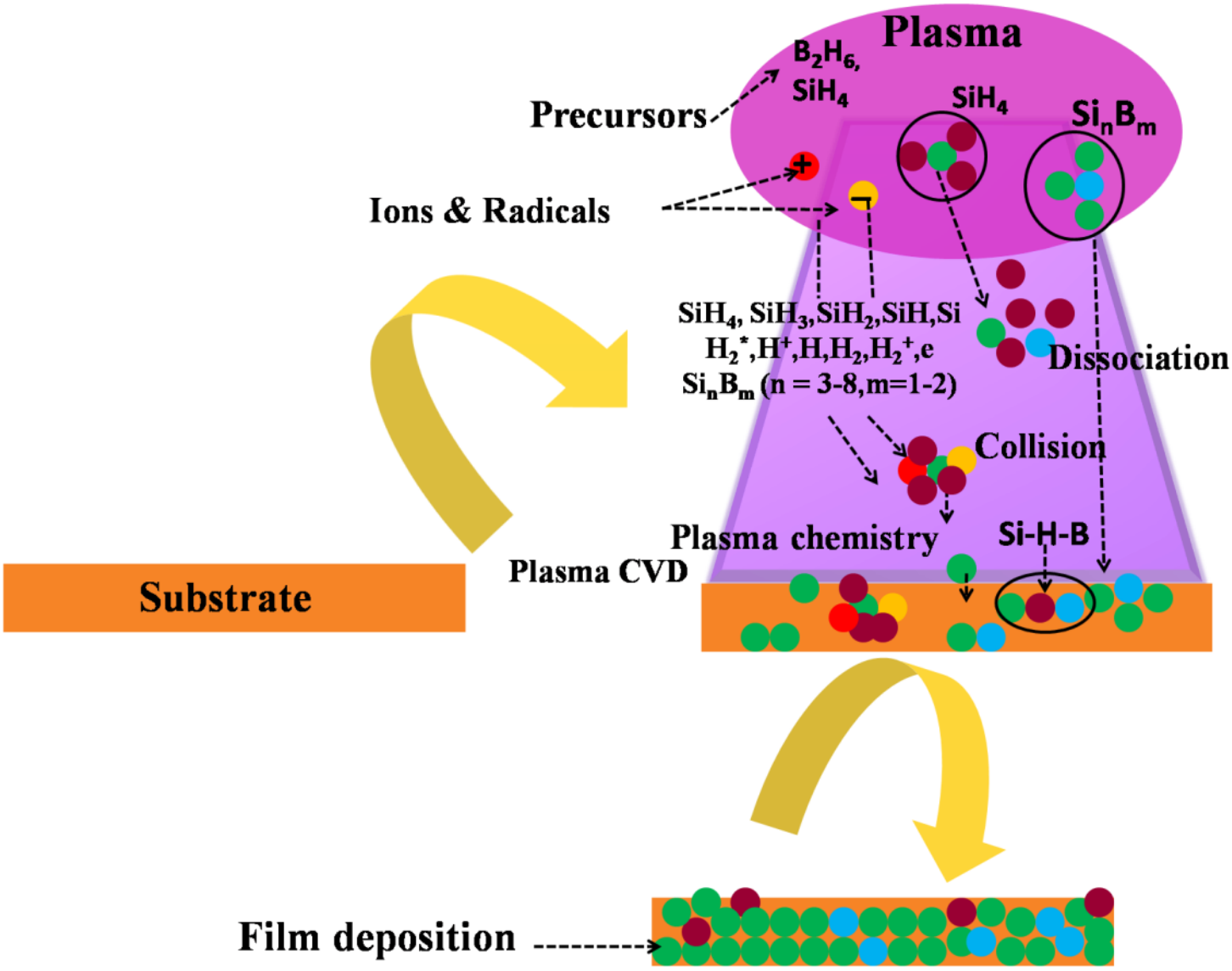

Figure 1

Schematic representation of steps of boron doped plasma chemistry and deposition of silicon film on the substrate.

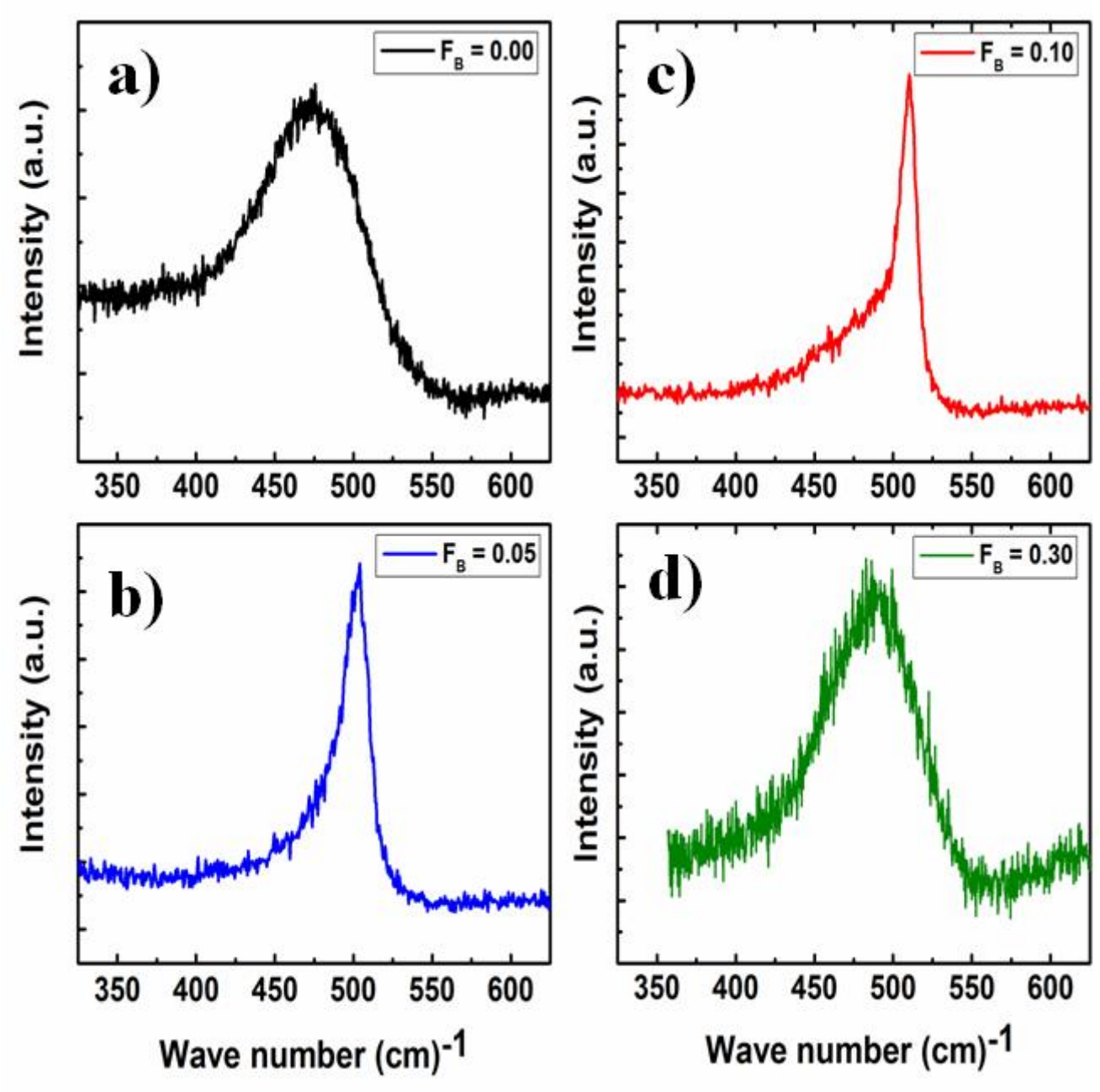

Figure 2

Raman spectra of p-type silicon films at varied diborone flow rate.

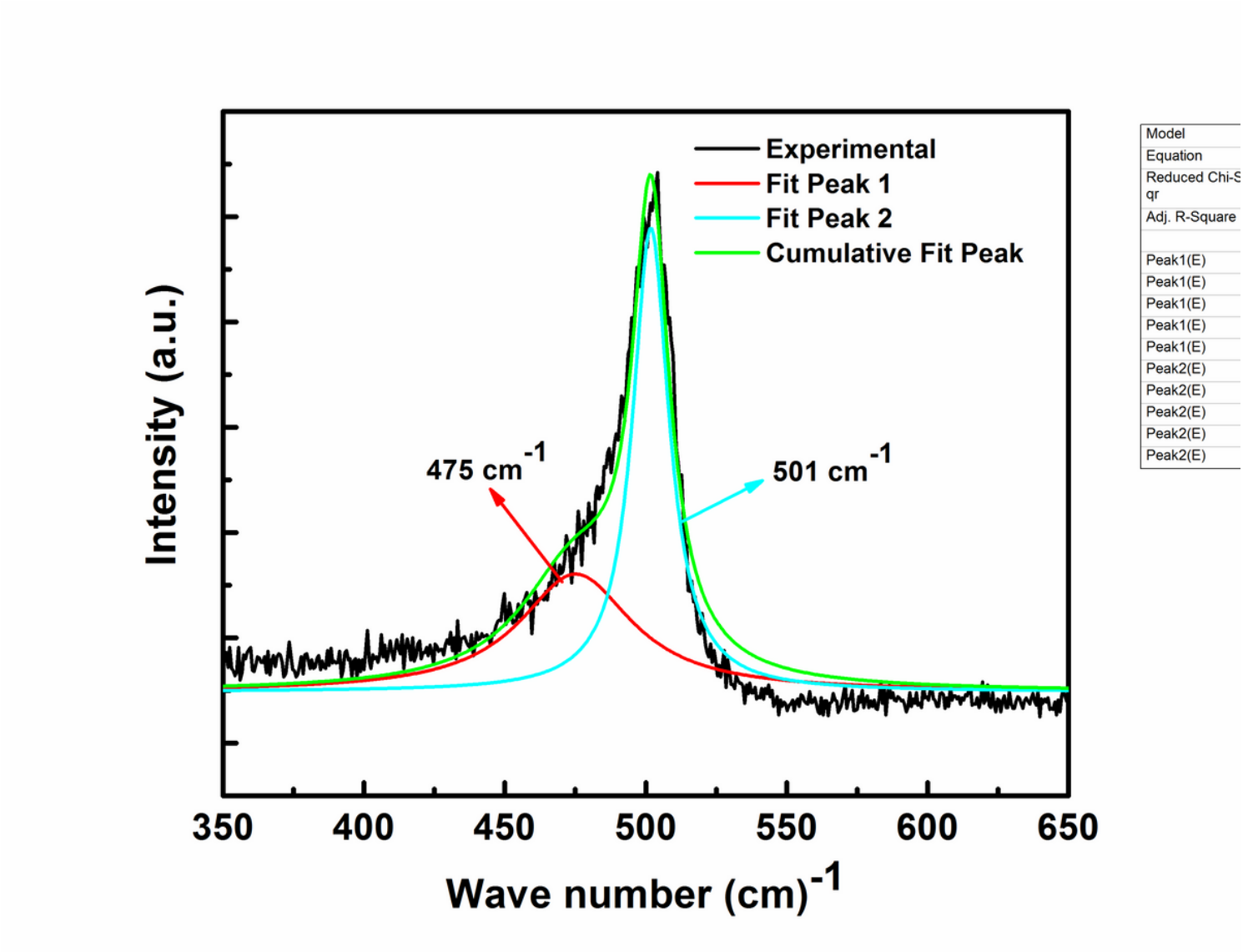

Figure 3

Deconvoluted Raman spectra at FB = 0.05

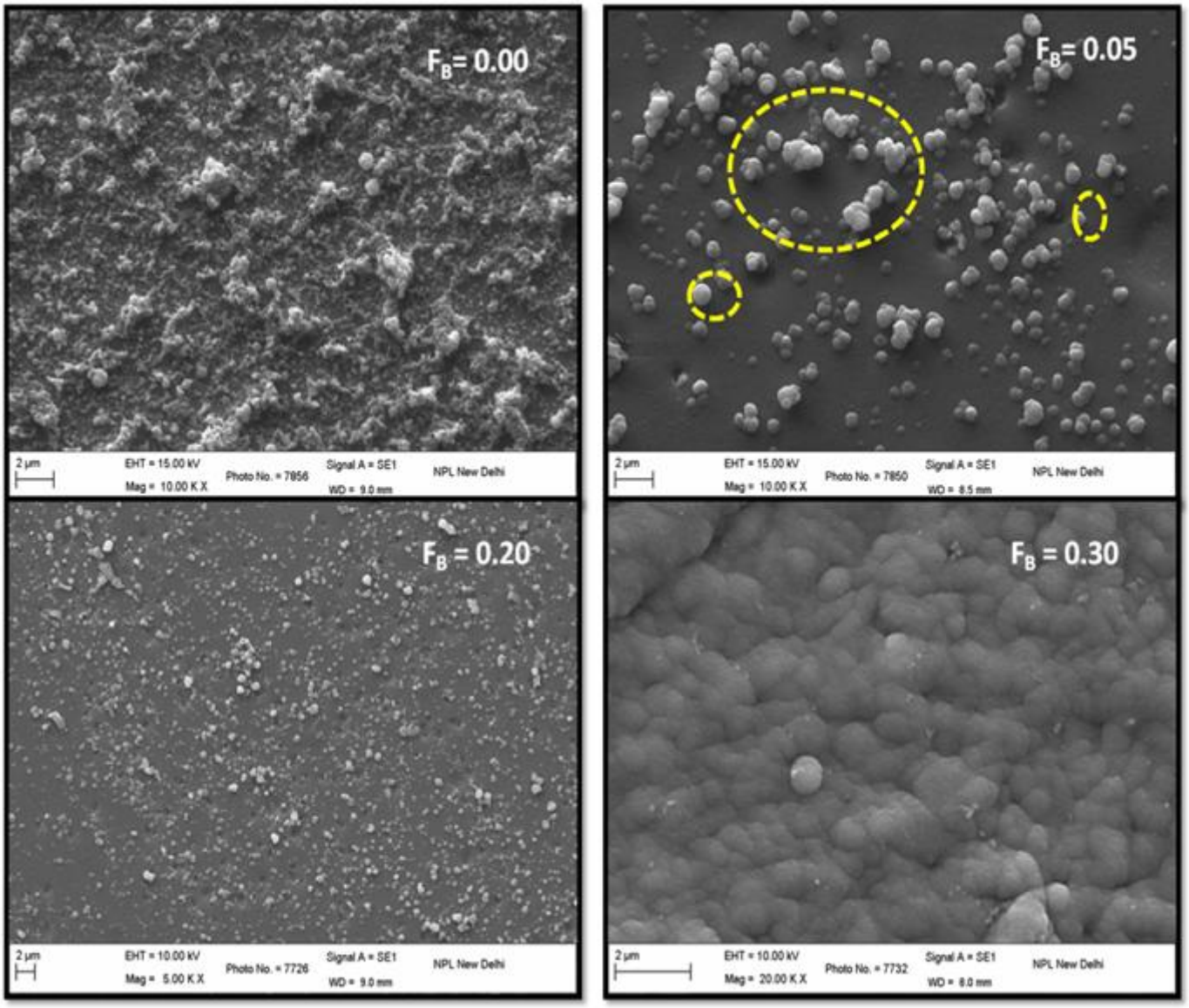

Figure 4

FE-SEM images of doped silicon thin films

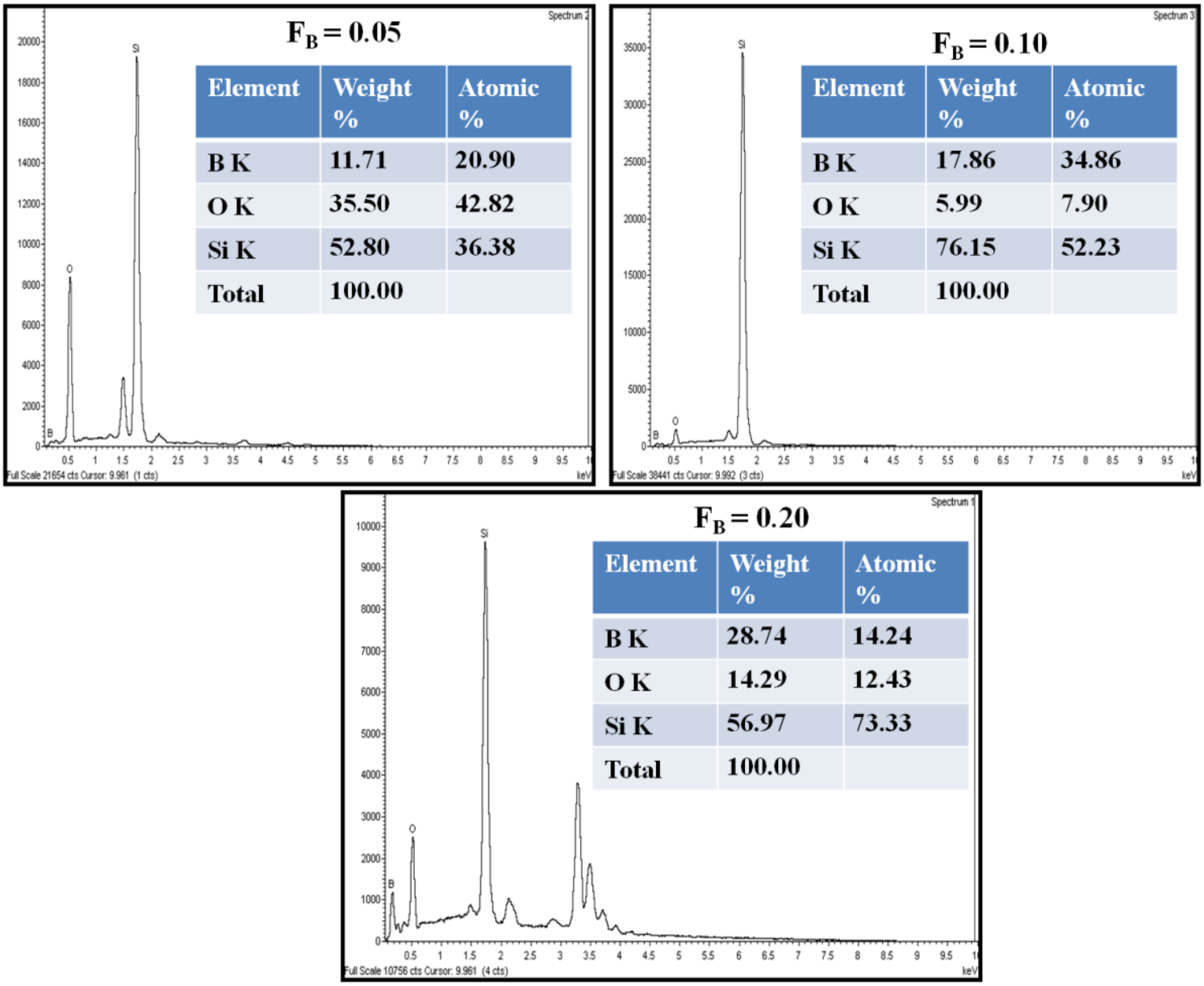

Figure 5

EDX spectra of diborane doped silicon films at different diborane doping

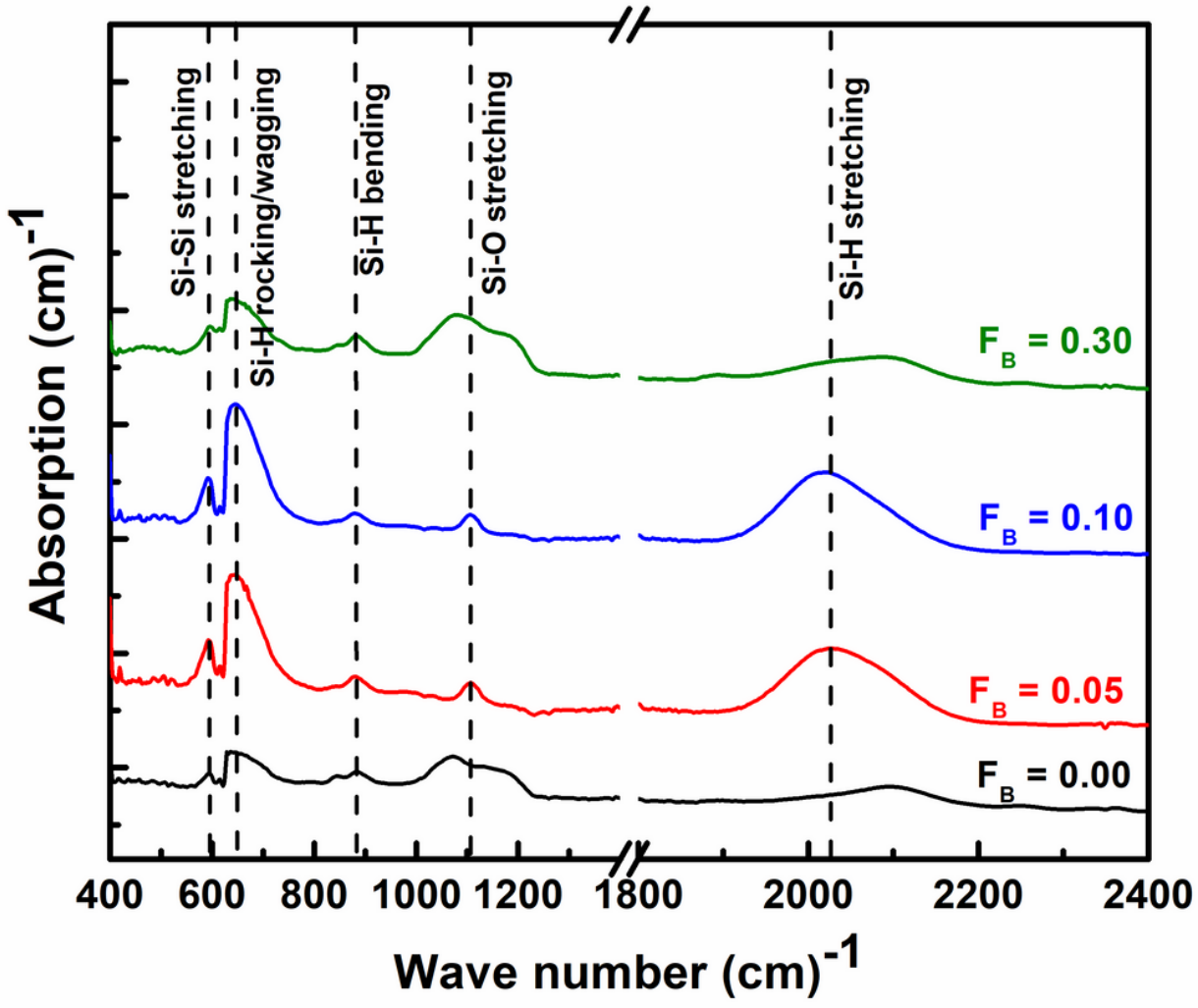

Figure 6

represents the FTIR spectra of boron doped silicon films

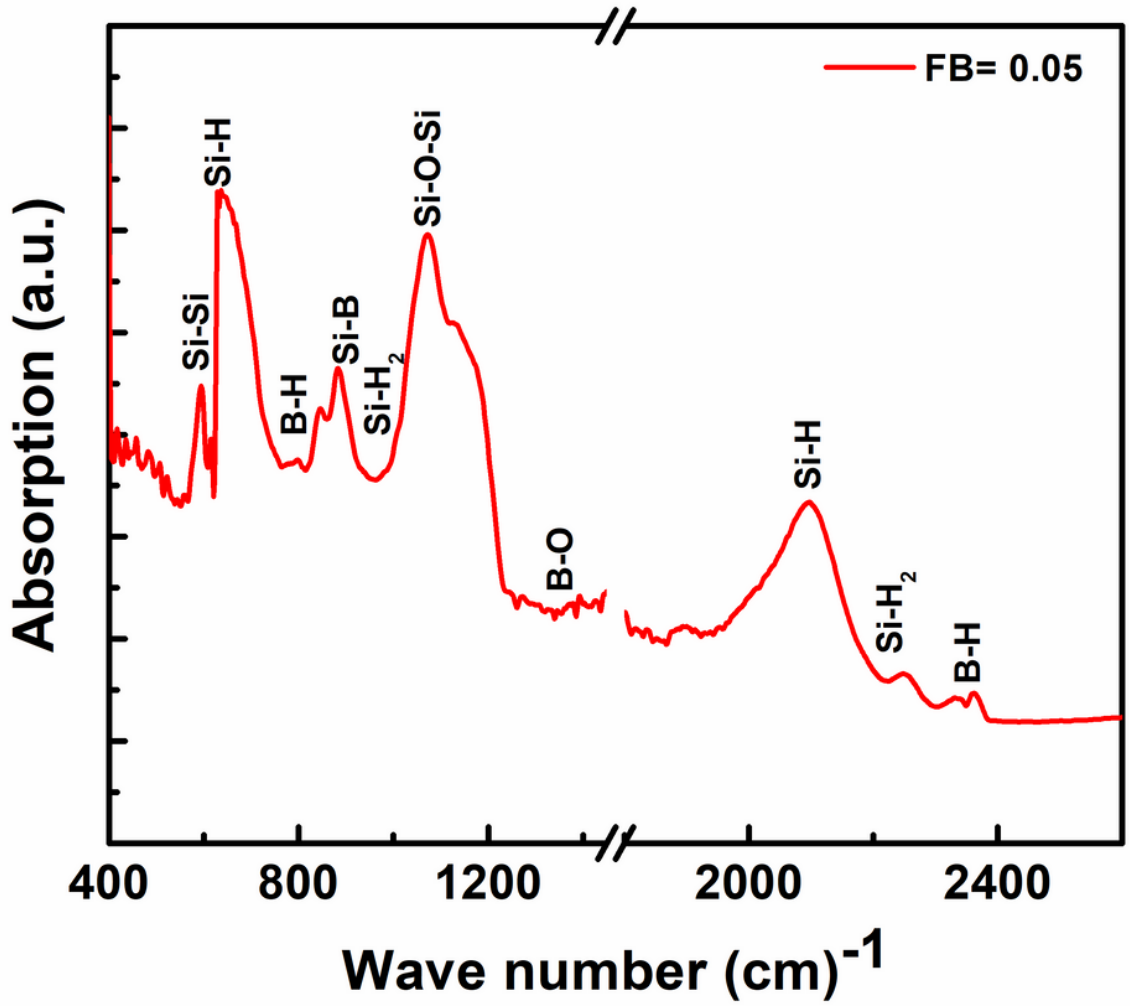

Figure 7

represents spectra of boron doped film deposited at FB = 0.05%.

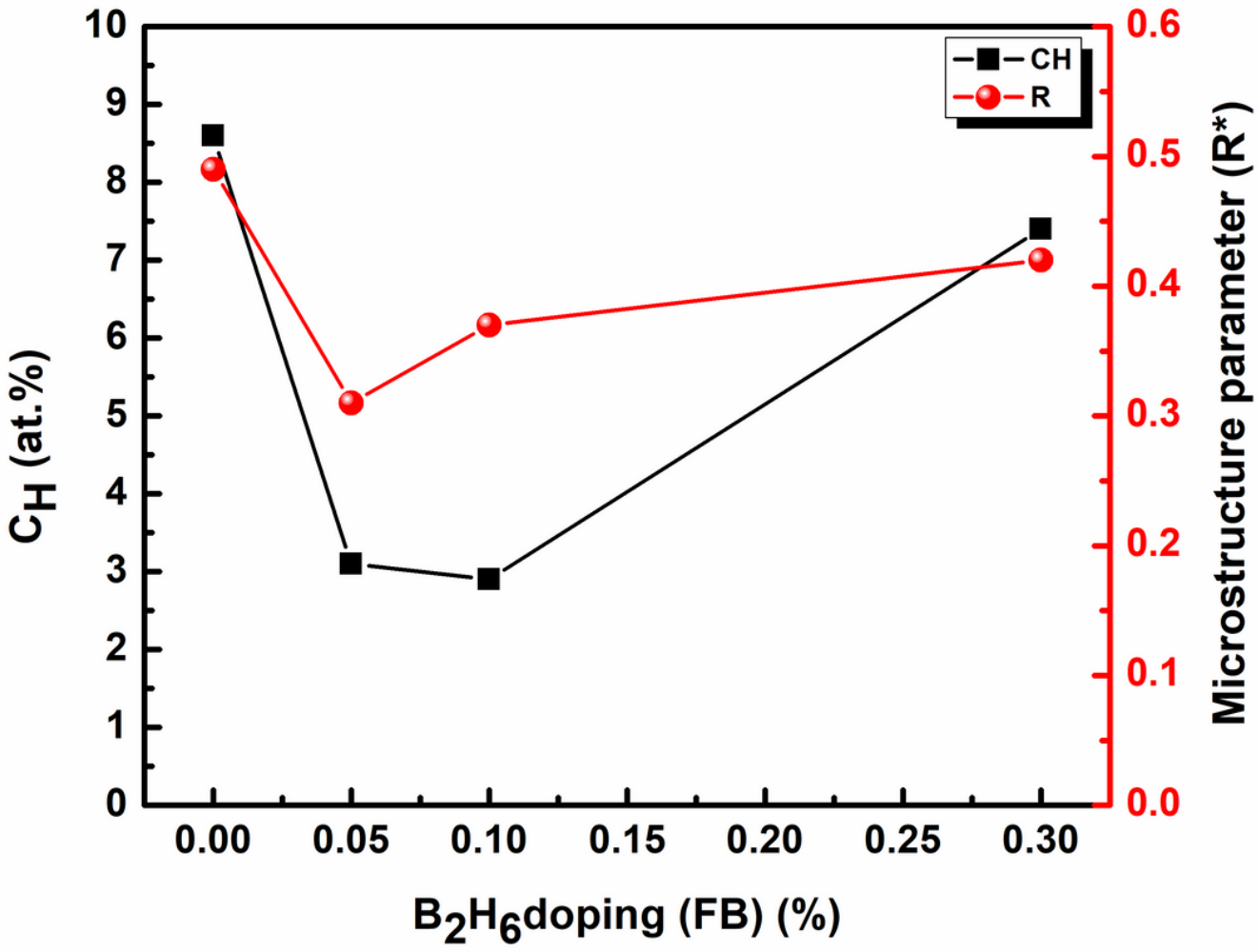

Figure 8

Estimation of hydrogen content and microstructure parameter represents the estimated hydrogen content and microstructure parameter as a function of different diborane gas flow.